Dalton Transactions

RSC Publishing

PERSPECTIVE

Catalysis science of supported vanadium oxide catalysts

Cite this: *Dalton Trans.*, 2013, **42**, 11762

Israel E. Wachs*

Supported vanadium oxide catalysts contain a vanadium oxide phase deposited on a high surface area oxide support (*e.g.*, Al_2O_3, SiO_2, TiO_2, *etc.*) and have found extensive applications as oxidation catalysts in the chemical, petroleum and environmental industries. This review of supported vanadium oxide catalysts focuses on the fundamental aspects of this novel class of catalytic materials (molecular structures, electronic structures, surface chemistry and structure–reactivity relationships). The molecular and electronic structures of the supported vanadium oxide phases were determined by the application of modern *in situ* characterization techniques (Raman, IR, UV-vis, XANES, EXAFS, solid state ^{51}V NMR and isotopic oxygen exchange). The characterization studies revealed that the supported vanadium oxide phase consists of two-dimensional surface vanadia sites dispersed on the oxide supports. Corresponding surface chemistry and reactivity studies demonstrated that the surface vanadia sites are the catalytic active sites for oxidation reactions by supported vanadia catalysts. Combination of characterization and reactivity studies demonstrate that the oxide support controls the redox properties of the surface vanadia sites that can be varied by as much as a factor of $\sim 10^3$.

Received 12th March 2013,
Accepted 11th April 2013

DOI: 10.1039/c3dt50692d

www.rsc.org/dalton

Operando Molecular Spectroscopy and Catalysis Laboratory, Department of Chemical Engineering, Lehigh University, Bethlehem, PA 18015, USA. E-mail: iew0@lehigh.edu; Tel: +1-610-758-4274

Israel E. Wachs

Israel E. Wachs studied chemical engineering at City College of the City University of New York and Stanford University. After several years at Exxon, he joined Lehigh University's Department of Chemical Engineering where he is the G. Whitney Snyder endowed professor and director of the Operando Molecular Spectroscopy and Catalysis Laboratory. He received awards for his research on the determination of electronic and molecular structures of catalytic active sites and their relationship to specific catalytic activity/selectivity (ACS Olah Award in Hydrocarbon or Petroleum Chemistry, AIChE Catalysis and Reaction Engineering Practice Award, EPA Clean Air Excellence Award, Humboldt Award, Vanadis Award).

I. Introduction

Supported vanadium oxide catalysts contain a vanadium oxide phase deposited on a high surface area oxide support (*e.g.*, Al_2O_3, SiO_2, TiO_2, *etc.*) and have found extensive applications as oxidation catalysts in the chemical, petroleum and environmental industries. The oxidation of sulfur dioxide to sulfur trioxide by vanadium oxide catalysts in the production of sulfuric acid, discovered by R. Meyers in 1899, has become the most significant vapor phase oxidation process in terms of annual production quantity.[1,2] The catalyst consists of a vanadium pentoxide alkali sulfate–pyrosulfate viscous melt on a SiO_2-based substrate. A similar type of catalyst was commercialized in 1916 for the oxidation of naphthalene, derived from coal liquids, to phthalic anhydride.[3] The availability of abundant and inexpensive *o*-xylene in the 1960s as a substitute for naphthalene for the production of phthalic anhydride, initiated research programs to discover catalysts that could selectively oxidize *o*-xylene to phthalic anhydride. This research effort culminated in the discovery of supported V_2O_5/TiO_2 catalysts, consisting of a two-dimensional surface vanadium oxide phase strongly interacting with the titania support (sometimes referred to as "monolayer catalysts"), that represents a new class of catalytic materials.[3,4] The focus of this review is not the supported vanadium pentoxide alkali sulfate–pyrosulfate liquid phase catalysts, but supported vanadium oxide monolayer catalysts.[4,5]

The discovery that supported V_2O_5/TiO_2 catalysts have excellent oxidation characteristics for *o*-xylene oxidation to phthalic anhydride lead within a short period to the application of such catalysts, *e.g.*, supported V_2O_5/Al_2O_3 and V_2O_5/TiO_2, catalysts for selective oxidation of alkyl pyridines to nicotinic acid (pyridine-3-carboxylic acid) and its derivatives in the manufacture of the vitamin B complex[3] and selective catalytic reduction (SCR) of NO_x emissions with ammonia or urea from power plants.[2] The supported V_2O_5/TiO_2 catalysts have also been found to possess other desirable oxidation properties for power plant emissions (*e.g.*, oxidative destruction of chlorinated hydrocarbons[6] and oxidation of elemental mercury to mercury oxides that are easier to trap[7]). This new class of supported vanadium oxide catalysts has also been extensively investigated for numerous selective oxidation catalytic reactions over the years.[7] This review of supported vanadium oxide catalysts focuses on the fundamental aspects of this novel class of catalysts (molecular structures, electronic structures, surface chemistry, and structure–reactivity relationships).

II. Nature of supported vanadium oxide phase in supported vanadium oxide catalysts: 3D particle or surface phase?

Fundamental research on the nature of the supported vanadium oxide phase on the titania support began in the 1970s, but there was no consensus among the researchers. Some researchers proposed that the supported vanadium oxide phase is present as crystalline V_2O_5 particles,[8,9] analogous to a supported metal on a high surface area oxide or as $V_xTi_{1-x}O_2$ solid solution,[10] while others proposed that it is present as a surface metal oxide monolayer (see Fig. 4).[11–14] This issue was finally resolved in 1985 with experiments that combined Raman spectroscopic characterization of the nature of the supported vanadia phase and the catalytic activity for *o*-xylene oxidation.[15] The Raman characterization revealed that the supported vanadia phase is present as surface vanadium oxide species below monolayer coverage and also forms crystalline V_2O_5 particles above monolayer coverage. The corresponding *o*-xylene oxidation catalytic properties demonstrated that the surface vanadium oxide phase is responsible for the overall catalytic activity and selectivity and that the crystalline V_2O_5 phase only has a minimal effect on the catalytic performance. Subsequent studies demonstrated that the formation and destruction of the surface vanadium oxide phase are directly related to the activation and deactivation of the supported vanadia catalyst, respectively.[16]

III. Molecular structure of the surface vanadium oxide phase under hydrated conditions

Under ambient conditions, hydrophilic oxide surfaces are saturated with moisture from humidity present in the air and the surface vanadia phase is solvated by moisture.[17] The aqueous phase equilibrium chemistry of vanadium oxide is well documented and vanadia's coordination chemistry is a function of both the concentration of vanadium and pH of the solution as shown in Fig. 1.[18] For high concentrations of vanadium in aqueous solution, the vanadia species continuously polymerize as the pH is lowered: $[VO_4]^{3-} \rightarrow [V_2O_7]^{2-} \rightarrow [V_4O_{12}]^{4-} \rightarrow [V_{10}O_{27}(OH)]^{5-} \rightarrow V_2O_{5(c)}$ precipitate. This exact same hydrated vanadium oxide species and equilibrium dependence on pH are also followed by the hydrated supported vanadia phase on oxide supports under ambient conditions.[19] The pH of thin aqueous films on oxide supports is determined by the pH at the point of zero charge (PZC), the pH where the number of surface protonated $(-OH_2)^+$ and deprotonated $(-O)^-$ sites are equal.[20] The pH at PZC values for several common oxide supports are presented in Table 1 and the pH at PZC for V_2O_5 is ~1.5. The much lower pH at PZC for V_2O_5 than the oxide supports results in an overall pH at PZC under ambient conditions that is intermediate between that of the oxide support and the supported vanadia phase, which can qualitatively be represented by the equation

$$\text{pH at PZC}(V_2O_5/\text{Support}) \sim [\text{pH at PZC}(\text{Support}) + \text{pH at PZC}(V_2O_5)]/2 \quad (1)$$

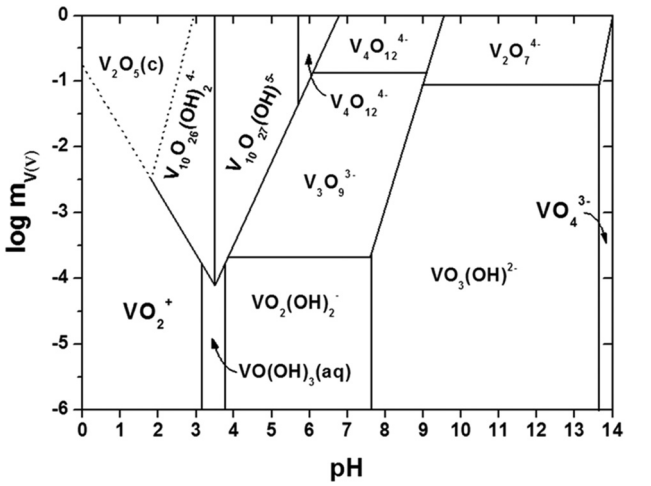

Fig. 1 Aqueous phase equilibrium chemistry of vanadium oxide as a function of both the concentration of vanadium and pH of the solution. This qualitative reproduction is based on the original diagram found in ref. 18.

Table 1 pH at PZC values for several common oxide supports

Oxide support	Surface pH
MgO	11
Al_2O_3	8.9
ZrO_2	5.9–6.1
TiO_2	6.0–6.4
SiO_2	2–4

The overall pH at PZC (V_2O_5/Support) is also dependent on the amount of vanadium oxide in the supported vanadia phase since the pH at PZC continuously decreases with increasing surface vanadia coverage.[21]

Although many claims in the catalysis literature have been made that the vanadium precursor and preparation method can affect the nature of the supported vanadium oxide phase, the equilibrium dependence of the hydrated surface vanadia species does not support this conclusion. Especially given that all supported vanadium oxide catalysts are exposed to ambient moisture after preparation. This has been experimentally confirmed for supported V_2O_5/TiO_2 catalysts synthesized by equilibrium adsorption, V-alkoxide, V-oxalate and grafting of VOC_3l.[22] Thus, the coordination of the hydrated surface vanadium oxide species are thermodynamically controlled and cannot be controlled by the specific V-precursor or preparation methods.

IV. Nature of the surface vanadium oxide phase under dehydrated conditions

Under dehydrated conditions, the supported vanadia catalyst is heated in dry air or an inert environment that desorbs the condensed moisture from the catalyst surface. The vibrational Raman spectra of crystalline V_2O_5 and the supported V_2O_5/Al_2O_3 catalyst under hydrated and dehydrated conditions are shown in Fig. 2. Crystalline V_2O_5 gives rise to sharp bands reflecting its ordered lattice structure. The sharp Raman band at 995 cm^{-1} arises from vibration of the vanadyl V=O bond and the remaining bands from 200–800 cm^{-1} are related to various vibrations of bridging V–O–V bonds of crystalline V_2O_5.[23] In contrast to the sharp Raman bands of crystalline V_2O_5, the supported vanadia catalysts do not exhibit the bands of crystalline V_2O_5 and possess broad bands reflecting the absence of long range order. The major Raman band for the hydrated supported V_2O_5/Al_2O_3 catalyst is centered at ~980 cm^{-1} that corresponds to hydrated $[V_{10}O_{27}(OH)]^{5-}$ decavanadate clusters.[19] The Raman spectrum of the dehydrated supported V_2O_5/Al_2O_3 is completely different than that for the corresponding hydrated catalyst indicating that there has been a structural change in the supported vanadium oxide phase upon dehydration. The Raman spectrum of the dehydrated supported V_2O_5/Al_2O_3 catalyst contains a new strong band at ~1025 cm^{-1} that is characteristic of a very short V=O bond and the broad band centered at ~900 cm^{-1} is related to the bridging V–O–Al bond that anchors the surface vanadia species to the alumina support.[24] The anchoring bonds are formed by condensation of V–OH and Al–OH bonds with titration of the Al–OH bonds directly observable with *in situ* IR spectroscopy.[25] The reversible nature of the dehydration/hydration supported vanadia phase directly confirms that the supported vanadia phase is present as a two-dimensional surface vanadia phase.

The influence of surface vanadia coverage upon the Raman spectra of the dehydrated supported V_2O_5/ZrO_2 catalyst system is presented in Fig. 3. At low vanadia loading, only the Raman band at 1025 cm^{-1} from the vanadyl V=O bond of the surface vanadia species is present and this band linearly increases in intensity with vanadia loading up to 4% V_2O_5/ZrO_2. The associated anchoring V–O–Zr Raman band is not as strong as that of the bridging V–O–Al band, but can readily be seen at ~950 cm^{-1} at high vanadia loading. Above 4% V_2O_5/ZrO_2, an additional band is present at 995 cm^{-1} related to the presence of crystalline V_2O_5 NPs, which further grows with additional vanadium oxide loading. The formation of crystalline V_2O_5 NPs suggests that the surface vanadia monolayer on ZrO_2 is saturated at ~4% V_2O_5/ZrO_2 and that introduction of additional vanadium oxide results in the formation of V_2O_5 NPs that reside on top of the surface vanadia monolayer. This is schematically represented in Fig. 4. Extensive detailed studies with numerous supported vanadium oxide catalyst systems revealed that monolayer surface vanadia coverage on oxide supports is usually achieved at ~8 V nm^{-2}.[25] An exception to this value for the surface vanadia monolayer coverage

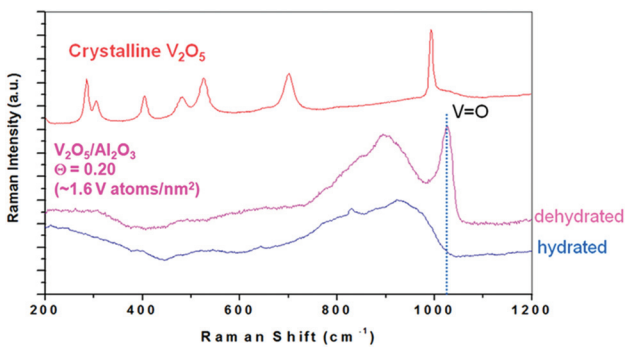

Fig. 2 *In situ* Raman spectroscopy of crystalline V_2O_5 and a supported V_2O_5/Al_2O_3 catalyst under hydrated and dehydrated conditions.

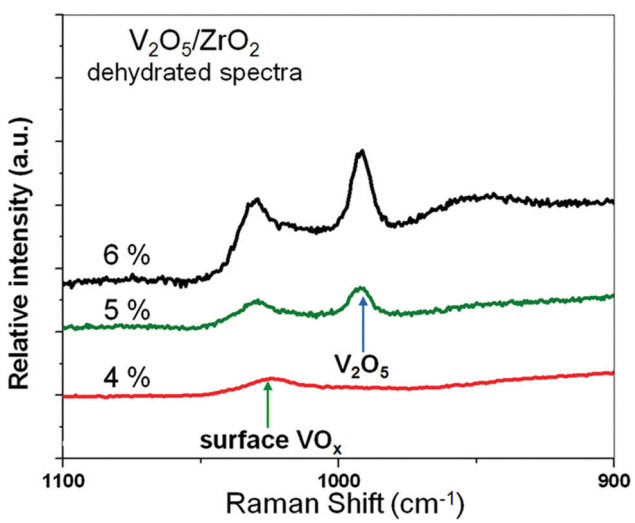

Fig. 3 *In situ* Raman spectroscopy of supported V_2O_5/ZrO_2 catalysts under dehydrated conditions.

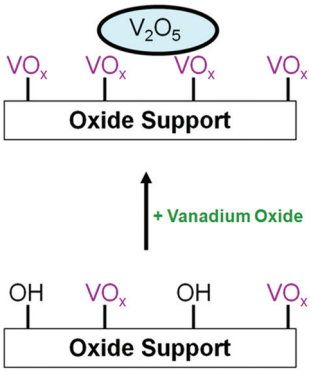

Fig. 4 Schematic representation of V_2O_5 nanoparticle formation on top of a surface vanadia monolayer with increasing vanadium oxide loading.

occurs for the supported V_2O_5/SiO_2 catalyst (~2.7 V nm^{-2}) because of the lower reactivity of the surface hydroxyls on SiO_2 supports.[26]

The preferential formation of the surface vanadium oxide layer on oxide supports prior to formation of crystalline V_2O_5 NPs is a consequence of the surface mobility of vanadium oxide and the lower surface free energy of crystalline V_2O_5 (8–9 × 10^{-6} J cm^{-2}) relative to the oxide supports (Al_2O_3 ~ 68–70 × 10^{-6} J cm^{-2}; ZrO_2 ~ 59–80 × 10^{-6} J cm^{-2}; TiO_2 ~ 28–38 × 10^{-6} J cm^{-2}).[27,28] The surface mobility of vanadium oxide is a consequence of its low melting temperature (595 °C) and corresponding low Tammann temperature (~200 °C) where surface atoms begin to diffuse.[27,28] The higher surface free energy values of the oxide supports is related to their termination with surface hydroxyls while V_2O_5 preferentially terminate with V=O bonds. This driving force is so strong that even heating physical mixtures of crystalline V_2O_5 and oxide support powders results in complete transformation of the crystalline V_2O_5 into a surface vanadia layer on the oxide support as shown schematically in Fig. 5.[27–29] The mobility of vanadium oxide is further enhanced in reactive environments where gaseous molecules complex with vanadium oxide.[27,28,30]

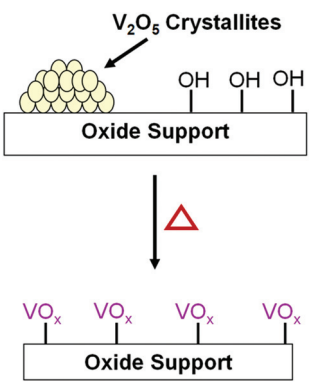

Fig. 5 Schematic representation of the formation of a surface vanadia monolayer by heating a physical mixture of crystalline V_2O_5 and oxide support powder (spontaneous dispersion).

V. Molecular structure of dehydrated surface vanadium oxide species on oxide supports

Determining the molecular structures of the surface vanadium oxide species was not straightforward since crystallographic techniques such as X-ray Diffraction (XRD) cannot detect the amorphous surface vanadia overlayer on oxide supports. Unlike XRD that requires long range order (>3 nm), X-ray Absorption Near Edge Spectroscopy (XANES) and solid-state ^{51}V NMR spectroscopy do not require long range order for their signals and are able to monitor the amorphous surface vanadia layer. The *in situ* XANES and solid-state ^{51}V NMR measurements showed that the dehydrated surface vanadia species are present in the V^{+5} oxidation state and possess VO_4 coordination.[17,31] Coupled *in situ* IR and Raman spectroscopy experiments, with the aid of isotopic ^{18}O labeling, demonstrated that the dehydrated surface VO_4 species have only one terminal V=O bond (mono-oxo structure).[32,33] *In situ* UV-vis and Raman spectroscopy revealed that both isolated and oligomeric surface VO_4 species are present on oxide supports.[34,35] The population of oligomeric surface vanadia species generally increases with surface vanadia coverage and the oligomers become the dominant species at high surface vanadia coverage.[35] An exception to this general trend occurs for supported V_2O_5/SiO_2 catalysts where only isolated surface VO_4 species are present due to the lower achievable surface vanadia coverage on silica.[26,35] A schematic of the isolated and polymeric surface vanadia species on oxide supports is shown in Fig. 6. There has been a recent claim[50] that surface dimeric V_2O_7 species may also be present on the SiO_2 support, but additional supporting experimental evidence for reference compounds possessing dimeric V_2O_7 units is required to substantiate this structural hypothesis. The coordination of the surface vanadia species was confirmed by the synthesis of model V–silsesquioxide complexes containing mono-oxo $O{=}V(-O-Si)_3$ sites that matched the solid-state ^{51}V NMR spectra of the supported vanadia catalysts.[36] Direct imaging of the surface vanadia species on a $CeO_2(111)$ support was recently successfully achieved with Scanning Tunneling Microscopy (STM).[37] These novel images conclusively show that the surface vanadia species possess mono-oxo surface VO_4 coordination that are presented as isolated and oligomeric species at low and high surface vanadia coverage, respectively.

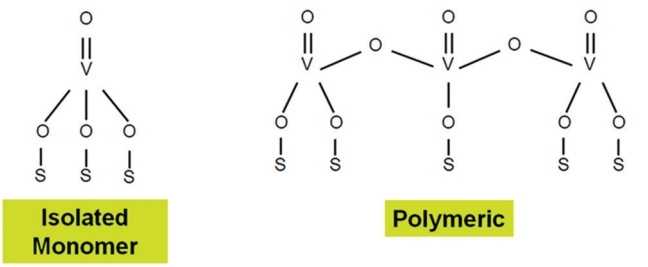

Fig. 6 Structures of surface VO_4 species found on metal oxide supports under dehydrated conditions.

VI. Surface chemistry of the surface vanadium oxide species

The surface vanadia species contain three types of oxygen atoms (V=O, V-Support and V–O–V) as shown in Fig. 6 and their interactions with CH_3OH were monitored with *in situ* Raman, IR and UV-vis spectroscopy.[38,39] Methanol adsorption on supported vanadia catalysts at ~120 °C proceeds by dissociative chemisorption to surface methoxy (CH_3O) and H at the bridging V–O-Support bond. The surface methoxy intermediate coordinates to the V site (C–H vibrations at 2832 and 2929 cm^{-1} and C–O–V vibration at 665 cm^{-1}) and the hydrogen atom reacts with the oxygen atom of the bridging V–O-Support to form a surface hydroxyl, Support-OH (see schematic in Fig. 7). Note that the surface vanadia site maintains its V^{+5} oxidation state during the dissociative chemisorption step because the oxygen atom of the surface methoxy intermediate replaces the original oxygen atom from the bridging V–O-Support bond.

The surface reactivity of the surface V–OCH_3 intermediate was investigated with CH_3OH-Temperature Programmed Surface Reaction (TPSR) spectroscopy. The CH_3OH-TPSR spectra are presented in Fig. 8 for the supported 5% V_2O_5/TiO_2 catalyst, which contains monolayer surface vanadia coverage, and reveal that the surface V–OCH_3 intermediate decomposes above 100 °C to yield formaldehyde (HCHO) and H_2O (evolution of water occurs at the same temperature and is not shown for brevity). The surface reaction kinetics are reflected in the temperature for maximum formation of formaldehyde (Tp, the peak temperature) as shown by Redhead.[40] The exact same surface kinetics, Tp value of 191 °C, is found whether the CH_3OH-TPSR experiment is performed in the presence of absence of gas phase molecular O_2. The independence of the surface kinetics for oxidation of the surface V–OCH_3 to HCHO and H_2O to the presence of gas phase molecular O_2 reveals that the oxygen involved in the rate-determining-step of the surface methoxy oxidation reaction is being supplied by the surface vanadia site and not by gaseous molecular O_2. This feature of methanol oxidation by supported vanadia catalysts indicates that the surface reaction kinetics proceed by the well-known Mars–van Krevelen mechanism whereby lattice oxygen is used for oxidation of the reactant and the function of gas phase molecular O_2 is only to replenish the oxygen removed by the reaction.[41] The dependence of the oxidation of the surface V–OCH_3 to formaldehyde on the oxygen associated with the surface vanadia site is further confirmed by CH_3OH-TPSR experiments where the surface vanadia species are partially reduced prior to chemisorption of methanol. The effect of partial pre-reduction of the surface vanadia species upon the CH_3OH-TPSR from supported V_2O_5/ZrO_2 is shown in Fig. 9 and pre-reduction results in both shifting of the Tp value of CH_3OH-TPSR to higher temperatures, reflecting decreased reaction rates, and reduction in the total amount of formaldehyde formed.[42,43] The CH_3OH-TPSR experiments demonstrate that the oxygen involved in the oxidation reaction step of surface V–OCH_3 to HCHO and water is associated with

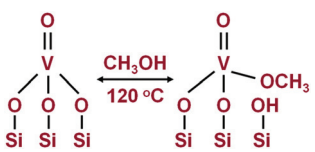

Fig. 7 Dissociative chemisorption of methanol on a surface vanadia site of supported vanadia catalysts.

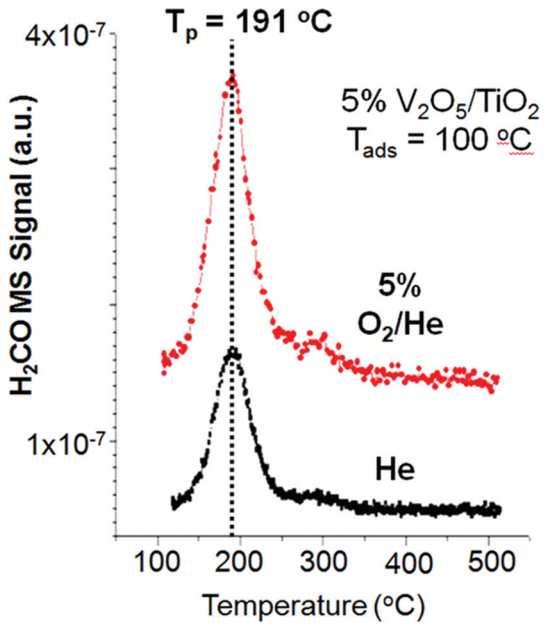

Fig. 8 Effect of gas phase molecular O_2 on the surface reaction kinetics of methanol to formaldehyde conversion during CH_3OH-TPSR by a supported 5% V_2O_5/TiO_2 catalyst.

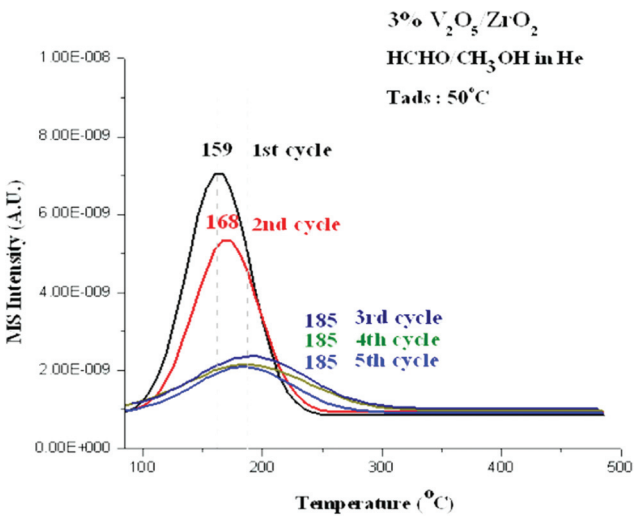

Fig. 9 Effect of partial pre-reduction of the surface vanadia species upon the CH_3OH-TPSR of the supported 3% V_2O_5/ZrO_2 catalyst. Pre-reduction achieved by performing sequential CH_3OH-TPSR experiments in flowing He without catalyst reoxidation. The 1st cycle corresponds to the fully oxidized catalyst.

the surface vanadia site and that the kinetics of this reaction is greatest for the fully oxidized surface vanadia site (V^{+5} >> V^{+4}/V^{+3}).

VII. Steady-state oxidation kinetics for supported vanadia catalysts

The steady-state kinetics for methanol oxidation by supported vanadia catalysts is independent of the partial pressure of gas phase molecular O_2 because of the direct participation of surface lattice oxygen associated with the surface vanadia site (rate ~ $[P_{O_2}]^0$). The steady-state methanol oxidation reaction kinetics over oxide catalysts is first-order in the partial pressure of methanol at low methanol concentrations (rate ~ $[P_{CH_3OH}]^1$) when the surface is not saturated with surface methoxy intermediates.[44] The steady-state methanol oxidation kinetics for methanol oxidation to formaldehyde as a function of vanadia loading for supported V_2O_5/Nb_2O_5 catalysts is shown in Fig. 10. In the absence of vanadia, the Nb_2O_5 support exhibits minimal catalytic activity for methanol oxidation to formaldehyde. Below monolayer surface vanadia coverage, where vanadia is 100% dispersed on the niobia support, the steady-state kinetics increases linearly with the number of surface vanadia sites. This linear trend reflects the first-order dependence of the methanol oxidation reaction on the surface concentration of surface vanadia sites (rate ~ $[(VO_4)_s]^1$) with the subscript s indicating the surface nature of the vanadia sites) and reveals that the surface vanadia sites are the catalytic active sites for methanol oxidation to formaldehyde. The linear dependence of the steady-state kinetics on $[(VO_4)_s]$ also indicates that the methanol oxidation reaction proceeds on only one surface VO_4 site. This is directly demonstrated by the plot of ln(rate) *vs.* ln$[(VO_4)_s]$ that yields a slope of 1. Above monolayer surface vanadia coverage, the steady-state catalytic activity decreases with increasing vanadia loading. As indicated above in section IV and the schematic in Fig. 4, crystalline V_2O_5 NPs form above monolayer coverage and reside on top of the surface vanadia sites. The decrease in overall activity above monolayer surface vanadia coverage indicates that the V_2O_5 NPs do not significantly contribute to the methanol oxidation reaction and actually block access of methanol to the surface vanadia sites.

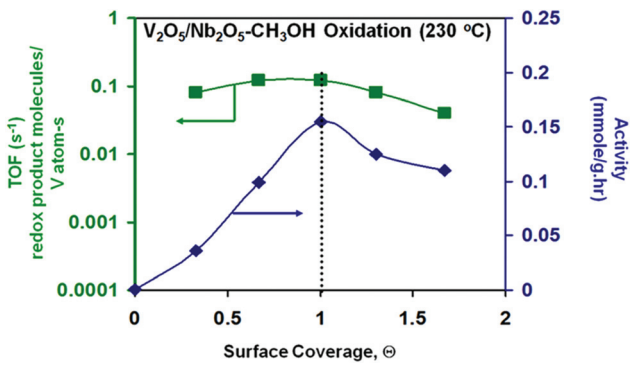

Fig. 10 Steady-state kinetics for methanol oxidation to formaldehyde as a function of vanadia loading for supported V_2O_5/Nb_2O_5 catalysts.

In the sub-monolayer region, the surface vanadia sites are isolated at low coverage and become oligomeric at high coverage (see above section V).[34,35] The relative contribution of isolated and polymeric surface vanadia sites to methanol oxidation can be determined from the specific steady-state turnover frequency per vanadia site (TOF: number of redox products formed/V atom-s) because the surface vanadia sites are 100% exposed below monolayer coverage. The relatively constant steady-state methanol oxidation TOF value with surface vanadia coverage in the sub-monolayer region demonstrates that the specific activity of isolated and polymeric surface VO_4 sites for methanol oxidation is comparable. This observation is a general trend also found for other supported vanadia catalyst systems[45,46] and suggests that the oxygen in the bridging V–O–V bond is not involved in the critical rate-determining-step of methanol oxidation to formaldehyde. Above monolayer coverage, the presence of the V_2O_5 NPs slightly decreases the apparent TOF because of their lower activity and fewer number of exposed vanadia sites.[45]

The steady-state methanol oxidation kinetics, however, are extremely sensitive to the specific oxide support that the surface VO_4 sites are coordinated. Changing the oxide support from SiO_2 to CeO_2 changes the specific TOF by as much as a factor of ~10^3 revealing the important kinetic role of the bridging V–O-Support bond upon the kinetics of methanol oxidation.[46] It has been proposed that the electronegativity of the oxide support cation affects the electron density of the oxygen in the bridging V–O-Support bond where greater electron density, corresponding to lower electronegativity of the oxide support cation, promotes the redox activity of this oxygen (Ce > Zr ~ Ti > Al > Si).[47] Recent DFT calculations for ethanol oxidation to acetaldehyde by supported vanadia catalysts have proposed that the redox activity induced by the oxide supports is related to the ease of oxygen defect formation enthalpy and suggest that the reducibility of the supported vanadia site can be used as a reactivity descriptor.[48,49] In other words, oxide supports that induce low oxygen defect formation enthalpy for the supported vanadia sites will exhibit lower steady-state apparent activation energy and higher reaction rates for oxidation reactions by supported vanadia catalysts.

VIII. Conclusions

Surface vanadium oxide phases represent a new class of catalytic materials that spontaneously form on oxide supports by self-assembly because of the lower surface free-energy of the supported vanadia system than physical mixtures of bulk V_2O_5 and oxide supports. Advances in the molecular and electronic characterization techniques in the past few decades have provided the understanding of the local structures of the surface vanadia sites on oxide supports. Under ambient conditions, hydrated vanadia clusters are present on oxide supports and

decompose upon dehydration. Under dehydrated conditions, the supported vanadia phases consist of isolated and polymeric surface VO_4 species in the sub-monolayer region and crystalline V_2O_5 NPs are also present above monolayer coverage. The surface VO_4 sites are the catalytic active sites for oxidation reactions by supported vanadia catalysts. Both isolated and polymeric surface VO_4 sites exhibit the same specific catalytic activity (TOF) and larger crystalline V_2O_5 NPs above monolayer coverage tend to be less active. The specific activity of the surface VO_4 sites is tunable by the oxide support cation that controls the redox properties of the surface VO_4 site. These insights allow for molecular engineering of supported vanadia catalysts by controlling the following parameters during the catalyst synthesis step: (i) number of catalytic active sites deposited on the oxide support in the sub-monolayer region (0–8 V nm^{-2}) and (ii) specific activity of the surface VO_4 sites by variation of the oxide support cation (factor of $\sim 10^3$).

Acknowledgements

The financial support of NSF (Grant CBET-0933294) and Department of Energy-Basic Energy Sciences (Grant DE-FG02-93ER14350) during the course of this work is gratefully acknowledged.

References

1 C. L. Thomas, *Catalytic Processes and proven Catalysts*, Academic Press, New York, 1970, 182–184.
2 R. J. Farrauto and C. H. Bartholomew, *Fundamentals of Industrial Catalytic Processes*, Chapman & Hall, London, 1997, 621–639.
3 K. Weissermel and H.-J. Arpe, *Industrial Organic Chemistry – Important Raw Materials and Intermediates*, Verlag Chemie, Weinheim, 1978, 335–339.
4 I. E. Wachs and B. M. Weckhuysen, *Appl. Catal., A*, 1997, **157**, 67.
5 *Appl. Catal., A*, 1997, **157**, Special Issue on Supported Vanadium Oxide Catalysts.
6 S. Lomnicki, I. Yeskendirov, Z. Xu, M. Waters and M. D. Amiridis, *Organohalogen Compd.*, 1999, **40**, 481.
7 K. Madsen, A. D. Jensen, J. R. Thogersen and F. Frandsen, A mechanistic study of mercury oxidation over SCR catalysts, *International Congress on Catalysis*, Munich, Germany (July 1–5, 2012).
8 A. Vejux and P. Courtine, *J. Solid State Chem.*, 1978, **123**, 93.
9 M. Inomata, K. Mori, A. Miyamoto, T. Ui and Y. Murakami, *J. Phys. Chem.*, 1983, **87**, 754.
10 G. C. Bond, J. Sarkany and G. D. Parfitt, *J. Catal.*, 1979, **5**, 476.
11 R. Grabowski, B. Grzybowksa, J. Haber and J. Sloczynski, *React. Kinet. Catal. Lett.*, 1975, **2**, 81.
12 F. Roozeboom, T. Fransen, P. Mars and P. J. Gellings, *Z. Anorg. Chem.*, 1979, **449**, 25.
13 R. Kozlowski, R. F. Pettifer and J. M. Thomas, *J. Phys. Chem.*, 1983, **87**, 5176.
14 S. S. Chan, I. E. Wachs, L. L. Murrell, L. Wang and W. K. Hall, *J. Phys. Chem.*, 1984, **88**, 5831.
15 I. E. Wachs, R. Y. Saleh, S. S. Chan and C. C. Chersich, *Appl. Catal.*, 1985, **15**, 339.
16 R. Y. Saleh, I. E. Wachs, S. S. Chan and C. C. Chersich, *J. Catal.*, 1986, **98**, 102.
17 H. Eckert and I. E. Wachs, *J. Phys. Chem.*, 1989, **93**, 679.
18 C. F. Baes Jr. and R. E. Mesmer, *The Hydrolysis of Cations*, Wiley, N.Y., 1970.
19 G. Deo and I. E. Wachs, *J. Phys. Chem.*, 1991, **95**, 5889.
20 G. A. Park, *Chem. Rev.*, 1965, **65**, 177.
21 F. J. Gil-Llambias, A. M. Escudy, J. L. G. Fierro and A. L. Agudo, *J. Catal.*, 1985, **95**, 520.
22 T. Machej, J. Haber, A. M. Turek and I. E. Wachs, *Appl. Catal.*, 1991, **70**, 115–128.
23 I. R. Beattie and T. R. Gilson, *J. Chem. Soc. A*, 1969, 2322.
24 N. Magg, B. Immaraporn, J. B. Giorgi, T. Schroeder, M. Baumer, J. Dobler, Z. Wu, E. Kondratenko, M. Cherian, M. Baerns, P. C. Stair, J. Sauer and H. J. Freund, *J. Catal.*, 2004, **226**, 88.
25 I. E. Wachs, *Catal. Today*, 1996, **27**, 437.
26 X. Gao, S. R. Bare, B. M. Weckhuysen and I. E. Wachs, *J. Phys. Chem. B*, 1998, **102**, 10842.
27 H. Knozinger and E. Taglauer, *Catalysis*, 1993, **10**, 1.
28 J. Haber, T. Machej and T. Czeppe, *Surf. Sci.*, 1985, **151**, 301.
29 J. Haber, T. Machej, E. M. Serwicka and I. E. Wachs, *Catal. Lett.*, 1995, **32**, 101.
30 C.-B. Wang, Y. Cai and I. E. Wachs, *Langmuir*, 1999, **15**, 1223.
31 T. Tanaka, H. Yamashita, R. Tsuchitani, T. Funabiki and S. Yoshida, *J. Chem. Soc., Faraday Trans. 1*, 1988, **84**, 2987.
32 C. Christiani, P. Forzatti and G. Busca, *J. Catal.*, 1989, **116**, 588.
33 E. L. Lee and I. E. Wachs, *J. Phys. Chem. C*, 2008, **112**, 6487.
34 M. A. Vuurman and I. E. Wachs, *J. Phys. Chem.*, 1992, **96**, 5200.
35 H. Tian, E. I. Ross and I. E. Wachs, *J. Phys. Chem. B*, 2006, **110**, 9593.
36 N. Das, H. Eckert, H. Hu, I. E. Wachs, J. F. Walzer and F. J. Feher, *J. Phys. Chem.*, 1993, **97**, 8240.
37 H.-J. Freund, *Chem.–Eur. J.*, 2010, **16**, 9384.
38 J.-M. Jehng, H. Hu, X. Gao and I. E. Wachs, *Catal. Today*, 1996, **28**, 335.
39 L. J. Burcham, G. Deo, X. Gao and I. E. Wachs, *Top. Catal.*, 2000, **11/12**, 85.
40 P. A. Redhead, *Vacuum*, 1962, **12**, 213.
41 P. Mars and D. W. van Krevelen, *Chem. Eng. Sci. Spec. Suppl.*, 1954, **3**, 41.
42 G. S. Wong, M. R. Concepcion and J. M. Vohs, *J. Phys. Chem. B*, 2002, **106**, 6451.
43 G. Wong and J. Vohs, *Surf. Sci.*, 2002, **498**, 266.

44 W. L. Holstein and C. J. Machiels, *J. Catal.*, 1996, **162**, 118.
45 T. Kim and I. E. Wachs, *J. Catal.*, 2008, **255**, 197.
46 G. Deo and I. E. Wachs, *J. Catal.*, 1994, **146**, 323.
47 I. E. Wachs, *Catal. Today*, 2005, **100**, 79.
48 B. Beck, M. Harth, N. G. Hamilton, C. Carrero, J. J. Uhlrich, A. Trunschke, S. Shaikhutdinov, H. Schubert, H.-J. Freund, R. Schlögl, J. Sauer and R. Schomäcker, *J. Catal.*, 2012, **296**, 120.
49 H. Y. Kim, H. M. Lee, R. G. S. Pala, V. Shapovalov and H. Metiu, *J. Phys. Chem. C*, 2008, **112**, 12398.
50 M. Cavalleri, K. Hermann, A. Knop-Gericke, M. Havecker, R. Herbert, C. Hess, A. Oestereich, J. Dobler and R. Schlogl, *J. Catal.*, 2009, **262**, 215.